Effect of defects in Heusler alloy thin films on spin-dependent tunnelling characteristics of $Co_2MnSi/MgO/Co_2MnSi$ and $Co_2MnGe/MgO/Co_2MnGe$ magnetic tunnel junctions

2010 J. Phys.: Condens. Matter 22 164212

(http://iopscience.iop.org/0953-8984/22/16/164212)

J. Phys.: Condens. Matter **22** (2010) 164212 (9pp) doi:10.1088/0953-8984/22/16/164212

Effect of defects in Heusler alloy thin films on spin-dependent tunnelling characteristics of Co_2MnSi/MgO/Co_2MnSi and Co_2MnGe/MgO/Co_2MnGe magnetic tunnel junctions

Masafumi Yamamoto, Takayuki Ishikawa, Tomoyuki Taira, Gui-fang Li, Ken-ichi Matsuda and Tetsuya Uemura

Division of Electronics for Informatics, Hokkaido University, N14, W9, Kita-ku, Sapporo 060-0814, Japan

E-mail: yamamoto@nano.ist.hokudai.ac.jp

Received 30 June 2009, in final form 29 December 2009
Published 30 March 2010
Online at stacks.iop.org/JPhysCM/22/164212

Abstract

Fully epitaxial magnetic tunnel junctions (MTJs) with Co-based Heusler alloy Co_2MnSi electrodes and a MgO tunnel barrier were fabricated with various values of Mn composition α for $Co_2Mn_\alpha Si$ in $Co_2Mn_\alpha Si$/MgO/$Co_2Mn_\alpha Si$ MTJs. The tunnel magnetoresistance (TMR) ratios at both 4.2 K and room temperature (RT) increased systematically with increasing α in $Co_2Mn_\alpha Si$ electrodes from Mn-deficient compositions ($\alpha < 1$) up to a certain Mn-rich composition ($\alpha > 1$), demonstrating high TMR ratios of 1135% at 4.2 K and 236% at RT for MTJs with Mn-rich $Co_2Mn_\alpha Si$ electrodes with $\alpha = 1.29$. Identically fabricated $Co_2Mn_\beta Ge_\delta$/MgO/$Co_2Mn_\beta Ge_\delta$ ($\delta = 0.38$) MTJs showed similar dependence of the TMR ratio on Mn composition β, demonstrating relatively high TMR ratios of 650% at 4.2 K and 220% at RT for $\beta = 1.40$. The Mn composition dependence of the TMR ratio at both 4.2 K and RT observed commonly for both Co_2MnSi/MgO/Co_2MnSi and Co_2MnGe/MgO/Co_2MnGe MTJs can be attributed to suppressed minority-spin in-gap states around the Fermi level for Mn-rich Co_2MnSi and Co_2MnGe electrodes.

(Some figures in this article are in colour only in the electronic version)

1. Introduction

Manipulation of the spin degree of freedom of the conduction electrons in an electron device, or spintronics, has been extensively studied recently [1, 2]. Half-metallic ferromagnets feature an energy gap for one spin direction (mostly the minority-spin band) at the Fermi level (E_F), which provides complete spin polarization at E_F [3]. Because they exhibit complete spin polarization at E_F, half-metallic ferromagnets are one of the key materials for ferromagnetic electrodes in spintronic devices [4]. Co-based Heusler alloys (Co_2YZ, where Y is usually a transition metal and Z is a main group element) are amongst the most extensively studied potentially half-metallic electrode materials. This is because half-metallicity is theoretically predicted for several of these alloys [5–7] and because they have high Curie temperatures, which are well above room temperature (RT) [8]. Co-based Heusler alloy thin films have been applied for spintronic devices, including magnetic tunnel junctions (MTJs) [9–15] and giant magnetoresistance devices [16–19], and for spin injection from ferromagnetic electrodes into semiconductors [20, 21].

We have recently proposed and developed fully epitaxial MTJs with either a Co_2YZ thin film as a lower electrode [12, 13, 22–24] or Co_2YZ thin films as both lower and upper electrodes [25, 26], and with a MgO barrier in

both cases, and demonstrated high tunnel magnetoresistance (TMR) ratios of up to 705% at 4.2 K and 182% at RT for fully epitaxial Co_2MnSi/MgO/Co_2MnSi MTJs [26–28]. Fully epitaxial MTJ layer structures with Co_2YZ thin films and a MgO barrier are advantageous for thoroughly utilizing the high spin polarizations of potentially half-metallic Co_2YZ electrodes in terms of (1) preparing structurally high-quality single-crystal Co_2YZ electrodes, (2) forming atomically flat and abrupt interfaces, and (3) ensuring that the interfacial region of the Co_2YZ lower electrode facing the MgO barrier is not oxidized [29, 30] by the deposition of MgO barriers by electron beam evaporation. Epitaxial MTJs with Co_2YZ electrodes and a MgO barrier also enable an enhancement of the tunnel conductance for the parallel magnetization configuration as a result of coherent tunnelling of electrons of the majority-spin Δ_1 channel [31–33].

Note that heterostructures consisting of a Heusler alloy upper electrode on a MgO tunnel barrier are common basic building blocks for Co_2YZ/MgO/Co_2YZ MTJs and for layer structures for spin injection from a Heusler alloy electrode with a high spin polarization into semiconductors through a MgO tunnel barrier [34]. Thus, the development of Co_2YZ/MgO/Co_2YZ MTJs and clarification of key factors that determine their spin-dependent tunnelling characteristics would also be useful for constructing highly efficient spin injection layer structures consisting of a semiconductor channel/MgO barrier/Heusler alloy upper electrode. In our previous papers [26–28], the film composition of the Co_2MnSi electrodes used in the Co_2MnSi/MgO/Co_2MnSi MTJs was $Co_2Mn_{0.91}Si_{0.93}$, which is slightly Co-rich with respect to the Mn composition (or slightly Mn-deficient with respect to the Co composition). Nonstoichiometry in Co_2YZ inevitably leads to the introduction of defects in the Co_2YZ host. The effect of defects in Co_2YZ on spin-dependent electronic structures has been investigated theoretically [35–41]. Picozzi *et al* predicted from first principles that half-metallicity in Co_2MnSi and Co_2MnGe is lost for Co_{Mn} antisites, where a Mn site is replaced by a Co atom because of the appearance of minority-spin in-gap states just near E_F, while half-metallicity is retained for Mn_{Co} antisites, where a Co site is replaced by a Mn atom [35].

In the present study, our purpose has been to experimentally clarify the effect of defects in Heusler alloy thin films of Co_2MnSi (CMS) and Co_2MnGe (CMG) possibly associated with nonstoichiometry on potentially half-metallic electronic structures. For this purpose, we investigate the TMR characteristics of CMS/MgO/CMS-MTJs (CMS-MTJs) and CMG/MgO/CMG-MTJs (CMG-MTJs) fabricated with various Mn composition values α and β in the $Co_2Mn_\alpha Si$ and $Co_2Mn_\beta Ge_\delta$ ($\delta = 0.38$) electrodes. We introduce formula unit composition models for the nonstoichiometric CMS and CMG taking into consideration the theoretically predicted formation energies for various kinds of defects for Co_2MnSi and Co_2MnGe [35, 41]. We then, on the basis of the formula unit composition models, discuss the origin of the Mn composition dependence of the TMR ratio at both 4.2 K and RT observed commonly for both CMS-MTJs and CMG-MTJs in terms of the effect of defects in the prepared CMS and CMG electrodes. We further examine the validity of the proposed formula unit composition model for the nonstoichiometric CMG films by investigating the saturation magnetization (μ_s) per formula unit (f.u.) as a function of β in the $Co_2Mn_\beta Ge_{0.38}$ electrodes.

This paper is organized as follows. Section 2 describes our experimental methods. Section 3 presents experimental results for the structural characterization and TMR characteristics of CMS-MTJs and CMG-MTJs fabricated with various Mn compositions for the $Co_2Mn_\alpha Si$ and $Co_2Mn_\beta Ge_\delta$ ($\delta = 0.38$) electrodes. Section 3 also presents the experimental saturation magnetization (μ_s) per formula unit (f.u.) of $Co_2Mn_\beta Ge_{0.38}$ thin films at 10 K for various β ranging from 0.67 to 1.40. Section 4 discusses a possible origin of the observed Mn composition dependence of the TMR ratio and μ_s in terms of the effects of defects possibly induced in nonstoichiometric CMS and CMG films. Section 5 summarizes our results and concludes.

2. Experimental methods

The fabrication procedure for CMS-MTJs and CMG-MTJs was essentially the same as in the case of the exchange-biased CMS-MTJs previously reported [26], but in this study we intentionally varied the Mn compositions in the CMS (CMG) electrodes by co-sputtering from a CMS (CMG) target and a Mn target for both the lower and upper CMS (CMG) electrodes. We used a nearly stoichiometric CMS target and a stoichiometric CMG target. We determined the film composition of the prepared CMS or CMG film through an inductively coupled plasma analysis with an accuracy of 2%–3% for each element, except Si, for which the accuracy was 5%. The film composition of the original CMS film prepared by sputtering from only a nearly stoichiometric CMS target was Mn-deficient $Co_2Mn_{0.69}Si_{1.01}$ and that of the original CMG film prepared by sputtering from only a stoichiometric CMG target was both Mn- and Ge-deficient $Co_2Mn_{0.67}Ge_{0.38}$. For CMS, the film composition was $Co_2Mn_\alpha Si_\gamma$ with $\gamma = 1.0 \pm 0.06$; i.e., the Co to Si ratio was almost 2:1. For CMG, the film composition was $Co_2Mn_\beta Ge_\delta$ with $\delta = 0.38$; i.e., Ge was strongly deficient. We prepared $Co_2Mn_\alpha Si_\gamma$ ($\gamma = 1.0 \pm 0.06$) electrodes with various values of α ranging from 0.69 to 1.46. We also prepared $Co_2Mn_\beta Ge_\delta$ ($\delta = 0.38$) electrodes with various values of β ranging from 0.67 to 1.40.

The fabricated MTJ layer structure was as follows: (from the substrate side) MgO buffer (10 nm)/CMS or CMG (both 30 nm)/MgO barrier (2–3 nm)/CMS (3 or 5 nm) or CMG (10 nm)/Ru (0.8 nm)/$Co_{90}Fe_{10}$ (2 nm)/$Ir_{22}Mn_{78}$ (10 nm)/Ru cap (5 nm), grown on a MgO(001) substrate. Each layer was successively deposited in an ultrahigh vacuum chamber (with a base pressure of about 6×10^{-8} Pa). The lower CMS (CMG) electrode was deposited at RT using magnetron sputtering and subsequently annealed *in situ* at 600 °C (500 °C) for 15 min. The MgO tunnel barrier was deposited by electron beam evaporation at RT. The deposition rate was 0.01 nm s^{-1} and the pressure during the deposition of the MgO tunnel barrier was about 6×10^{-7} Pa. We fabricated CMS-MTJs with different upper CMS electrode thicknesses

of 3 and 5 nm but typically 5 nm, and we fabricated CMG-MTJs with a fixed upper CMG electrode thickness of 10 nm. The upper CMS or CMG electrode was also deposited at RT. The MTJ trilayer was annealed *in situ* right after deposition of the upper CMS or CMG electrode at 550 °C for CMS-MTJs and 500 °C for CMG-MTJs. We fabricated MTJs with the layer structure described above using photolithography and Ar ion milling. The fabricated junction size was 10 μm × 10 μm. The magnetoresistance was measured with a magnetic field applied along the [110] axis of the Co_2YZ at 4.2 K and RT using a dc four-probe method. We defined the TMR ratio as $(R_{AP} - R_P)/R_P$, where R_P and R_{AP} are the respective resistances for the parallel (P) and antiparallel (AP) magnetization configurations between the lower and upper electrodes. The bias voltage (V) was defined with respect to the lower electrode; i.e., electrons tunnel from the lower Co_2YZ electrode to the upper Co_2YZ electrode at a positive V.

The magnetic properties of $Co_2Mn_\beta Ge_{0.38}$ thin films with various β ranging from 0.67 to 1.40 were measured by using a superconducting quantum interference device magnetometer (Quantum Design MPMS) at 10 K. For the estimation of magnetization, the contribution from the MgO substrate was subtracted. To obtain the μ_s values per f.u., the film thicknesses of $Co_2Mn_\beta Ge_{0.38}$ films were obtained through x-ray reflectivity measurements, and in-plane and perpendicular lattice constants, a and c, were measured by a θ–2θ scan with a four-circle x-ray diffractometer.

3. Experimental results

3.1. Structural properties

First, we describe the structural properties of the fabricated CMS-MTJ layer structures with co-sputtered CMS films having a film composition of $Co_2Mn_{1.29}Si_{1.06}$.

Sharp streak patterns dependent on the electron injection direction were obtained by reflection high energy electron diffraction (RHEED) for each successive layer in a CMS-MTJ trilayer structure with co-sputtered $Co_2Mn_{1.29}Si_{1.06}$ films, clearly indicating that all the layers, including the CMS lower electrode, MgO tunnel barrier, and CMS upper electrode, grew epitaxially. We also observed 1/2-order superlattice reflections along the $[110]_{CMS}$ direction in the RHEED patterns for both the lower CMS electrode annealed at 600 °C and the upper CMS electrode annealed at 550 °C, showing that both had the $L2_1$ structure.

Figure 1(a) shows a cross-sectional high-resolution transmission electron microscope (HRTEM) lattice image of an MTJ layer structure consisting of CMS (30 nm)/MgO barrier (2 nm)/CMS (5 nm)/Ru (0.8 nm)/$Co_{90}Fe_{10}$ (2 nm)/$Ir_{22}Mn_{78}$ (10 nm)/Ru cap (5 nm) with co-sputtered $Co_2Mn_{1.29}Si_{1.06}$ films, along the $[1\bar{1}0]$ direction of the CMS. This image clearly shows that all the layers of the CMS-MTJ trilayer were grown epitaxially and were single crystalline, as in the case of the MTJ layer structure with CMS films having a film composition of $Co_2Mn_{0.91}Si_{0.93}$ deposited from only a CMS target [28]. It also confirms that extremely smooth and abrupt interfaces were formed.

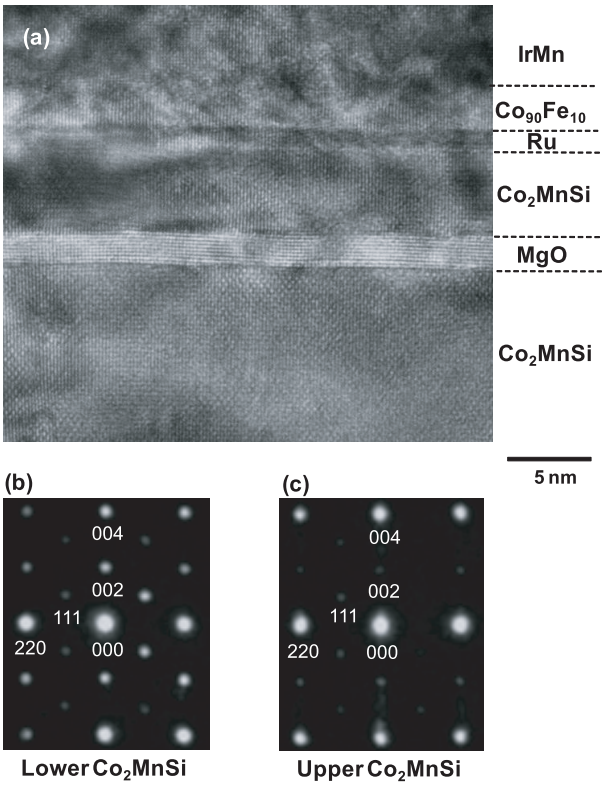

Figure 1. (a) Cross-sectional HRTEM lattice image of an MTJ layer structure consisting of CMS (30 nm)/MgO barrier (2 nm)/CMS (5 nm)/Ru (0.8 nm)/$Co_{90}Fe_{10}$ (2 nm)/$Ir_{22}Mn_{78}$ (10 nm)/Ru cap (5 nm) with CMS films with a film composition of $Co_2Mn_{1.29}Si_{1.06}$ grown on a MgO-buffered MgO substrate, along the $[1\bar{1}0]$ direction of the CMS, where the lower CMS electrode was annealed *in situ* at 600 °C after it was deposited at RT while the MTJ layer structure was annealed *in situ* at 550 °C after deposition of the upper electrode. (b) Electron diffraction pattern for the lower CMS electrode (30 nm). (c) Electron diffraction pattern for the upper CMS electrode (5 nm). The electron beam diameter was 2.5 nm.

Next, we describe the structural properties of CMS/Ru/$Co_{90}Fe_{10}$/IrMn quadrilayers. The cross-sectional HRTEM lattice image (figure 1(a)) showed that all the layers of Ru, $Co_{90}Fe_{10}$, and IrMn were grown epitaxially on the single-crystal CMS upper electrode and were single crystalline, as with fully epitaxial, exchange-biased Co_2YZ/MgO-based MTJs previously reported [13, 23, 24].

Figures 1(b) and (c) show micro-beam electron diffraction patterns for the lower and upper CMS electrodes for a beam diameter of 2.5 nm, where 111 spots were observed, indicating the $L2_1$ structure for both the lower and upper CMS thin films prepared by co-sputtering. It should be noted that both the 111 spots, which are characteristic of the $L2_1$ structure, and the 002 spots, which are characteristic of the B2 and $L2_1$ structures, are clearer for the lower CMS electrode than for the upper CMS electrode, although the same beam diameter of 2.5 nm was used for both the lower and upper electrodes. This difference in the superlattice spot intensities suggests that the degree of order for the upper CMS electrode is lower than that for the lower CMS electrode, which is common to that observed for lower and upper CMS electrodes previously prepared by sputtering from only a CMS target [42]. It should

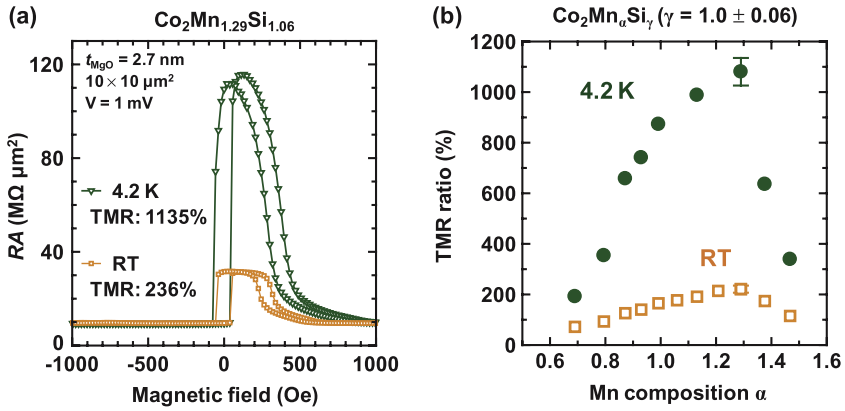

Figure 2. (a) Typical TMR curves at 4.2 K and RT for a CMS/MgO (2.7 nm)/CMS-MTJ with Mn-rich $Co_2Mn_{1.29}Si_{1.06}$ electrodes. The junction size was 10 μm × 10 μm. The bias voltage was 1 mV at both 4.2 K and RT. (b) TMR ratios at 4.2 K and RT for $Co_2Mn_\alpha Si_\gamma$/MgO/$Co_2Mn_\alpha Si_\gamma$ ($\gamma = 1.0 \pm 0.06$) MTJs as a function of α ranging from 0.69 (Mn-deficient CMS) to 1.46 (Mn-rich CMS). The bias voltages were 1 mV at 4.2 K and 5 mV at RT.

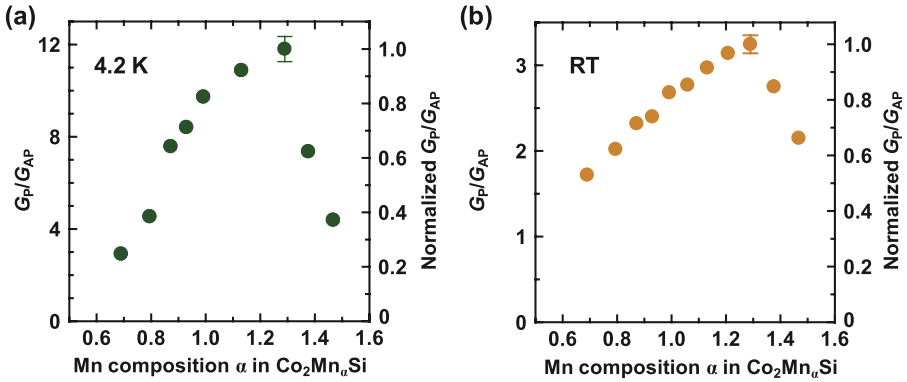

Figure 3. G_P/G_{AP} values at (a) 4.2 K and (b) RT that provided the TMR ratios (TMR ratio = $G_P/G_{AP} - 1$) shown in figure 2(b) for CMS-MTJs as a function of α. The right vertical axes show normalized G_P/G_{AP} values, where G_P/G_{AP} values were normalized by the respective mean values for $\alpha = 1.29$ at 4.2 K and RT.

also be noted that unknown spots were superimposed onto the Heusler $L2_1$ spots in some regions of the lower and upper CMS electrodes, indicating the coexistence of unidentified materials or structures in addition to the Heusler $L2_1$ structure. This was in contrast to the micro-beam electron diffraction patterns for CMS thin films used as both lower and upper electrodes with a film composition of $Co_2Mn_{0.91}Si_{0.93}$, which were deposited by sputtering with only a CMS target: those patterns showed only the $L2_1$ structure for any spot region [28].

Similarly, sharp streak patterns dependent on the electron injection direction were obtained for each successive layer in the CMG-MTJ trilayer structure with co-sputtered CMG films, clearly indicating that all the layers, including the CMG lower electrode, MgO tunnel barrier, and CMG upper electrode grew epitaxially (not shown).

3.2. Spin-dependent tunnelling characteristics of Co_2MnSi/MgO/Co_2MnSi MTJs as a function of Mn composition α in $Co_2Mn_\alpha Si$ electrodes

We now describe the TMR characteristics of CMS-MTJs with $Co_2Mn_\alpha Si_\gamma$ ($\gamma = 1.0 \pm 0.06$) electrodes fabricated with α ranging from 0.69 to 1.46. Hereafter, we denote $Co_2Mn_\alpha Si_\gamma$ ($\gamma = 1.0 \pm 0.06$) by $Co_2Mn_\alpha Si$ using the mean value of 1.0 for Si composition γ.

Typical TMR curves at 4.2 K and RT for a fabricated epitaxial CMS/MgO (2.7 nm)/CMS-MTJ with Mn-rich $Co_2Mn_{1.29}Si_{1.06}$ electrodes are shown in figure 2(a). The thickness of the upper CMS electrode was 3 nm. The bias voltage was 1 mV at both 4.2 K and RT. Clear exchange-biased TMR characteristics were obtained with high TMR ratios of 1135% at 4.2 K and 236% at RT. These values are significantly better than previously reported TMR ratios of 705% at 4.2 K and 182% at RT for a CMS-MTJ with slightly Mn-deficient $Co_2Mn_{0.91}Si_{0.93}$ electrodes prepared by sputtering with only a CMS target [26, 28].

Figure 2(b) shows the TMR ratios at 4.2 K and RT for CMS-MTJs as a function of α ranging from 0.69 to 1.46, where both the lower and upper CMS electrodes, except those with $\alpha = 0.69$, were deposited by co-sputtering. The bias voltages were 1 mV at 4.2 K and 5 mV at RT. (The lowering of the TMR ratios measured at 5 mV was negligibly small compared to those measured at 1 mV at RT.) The error bars for the TMR ratios for $\alpha = 1.29$ indicate the range of observed TMR

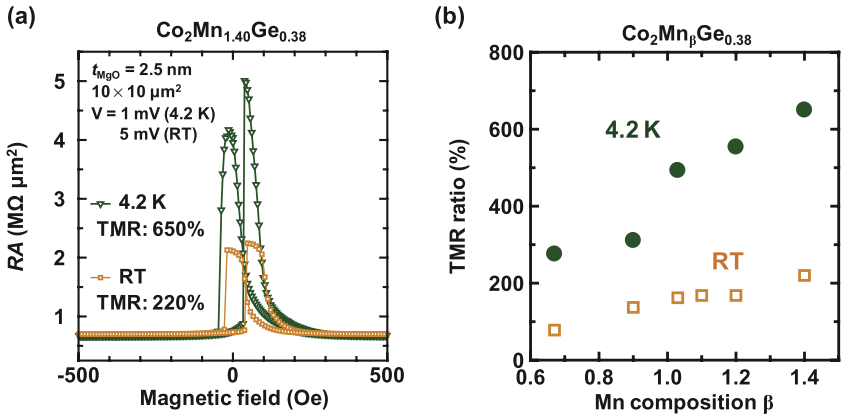

Figure 4. (a) Typical TMR curves at 4.2 K and RT for a CMG/MgO (2.5 nm)/CMG-MTJ with Mn-rich $Co_2Mn_{1.40}Ge_{0.38}$ electrodes. The junction size was 10 μm × 10 μm. (b) TMR ratios at 4.2 K and RT for $Co_2Mn_\beta Ge_{0.38}$/MgO/$Co_2Mn_\beta Ge_{0.38}$ MTJs as a function of β ranging from 0.67 (Mn- and Ge-deficient CMG) to 1.40 (Mn-rich and Ge-deficient CMG). The bias voltages were 1 mV at 4.2 K and 5 mV at RT for both (a) and (b).

ratios for MTJs fabricated with different upper CMS electrode thicknesses ($t_{upper-CMS}$) of 3 and 5 nm. We found that the TMR ratios at both 4.2 K and RT showed strong dependence on α. The TMR ratio at 4.2 K increased from 192% for Mn-deficient $\alpha = 0.69$ to 1135% for Mn-rich $\alpha = 1.29$. It then decreased for α beyond 1.29. Similarly, the TMR ratio at RT increased from 72% for Mn-deficient $\alpha = 0.69$ to 236% for Mn-rich $\alpha = 1.29$ and then decreased for α beyond 1.29.

Most importantly, the TMR ratios at both 4.2 K and RT increased with α even beyond $\alpha = 1.0$, where the film composition is close to the stoichiometric Co_2MnSi composition, and the maximum TMR ratios of 1135% at 4.2 K and 236% at RT were obtained for $\alpha = 1.29$. Thus, we experimentally found that the TMR ratios for CMS-MTJs with nonstoichiometric, Mn-rich Co_2MnSi electrodes with a film composition of $Co_2Mn_{1.29}Si_{1.06}$ were higher than those for MTJs with almost stoichiometric Co_2MnSi electrodes.

Figure 3 shows G_P/G_{AP} values at 4.2 K and RT that provided the TMR ratios (TMR ratio $= G_P/G_{AP} - 1$) shown in figure 2(b) for CMS-MTJs as a function of α, where $G_P = 1/R_P$ and $G_{AP} = 1/R_{AP}$ are the respective tunnel conductances for P and AP. The G_P/G_{AP} values at both 4.2 K and RT showed similar dependence on α; i.e., G_P/G_{AP} increased with increasing α from 0.69 to 1.29 and then decreased for α beyond 1.29 at both 4.2 K and RT. The origin of the dependence of the TMR ratio or equivalently of G_P/G_{AP} on α is discussed in section 4.

3.3. Spin-dependent tunnelling characteristics of Co_2MnGe/MgO/Co_2MnGe MTJs as a function of Mn composition β in $Co_2Mn_\beta Ge_{0.38}$ electrodes

Next, we describe the TMR characteristics of CMG-MTJs with $Co_2Mn_\beta Ge_{0.38}$ electrodes fabricated with β ranging from 0.67 (Mn-deficient CMG) to 1.40 (Mn-rich CMG). Figure 4(a) shows typical TMR curves at 4.2 K and RT for a CMG/MgO (2.5 nm)/CMG-MTJ with co-sputtered Mn-rich $Co_2Mn_{1.40}Ge_{0.38}$ electrodes. The bias voltages were 1 mV at 4.2 K and 5 mV at RT. Clear exchange-biased TMR characteristics were obtained with relatively high TMR ratios of 650% at 4.2 K and 220% at RT.

Figure 4(b) shows TMR ratios at 4.2 K and RT for CMG-MTJs as a function of β ranging from 0.67 to 1.40, where both the lower and upper CMG electrodes, except those with $\beta = 0.67$, were deposited by co-sputtering. The bias voltages were again 1 mV at 4.2 K and 5 mV at RT. As with the CMS-MTJs, the TMR ratios at both 4.2 K and RT showed strong dependence on β in $Co_2Mn_\beta Ge_{0.38}$. The TMR ratio at 4.2 K increased from 276% for Mn- and Ge-deficient $\beta = 0.67$ to 650% for Mn-rich and Ge-deficient $\beta = 1.40$. Similarly, the TMR ratio at RT increased from 78% for $\beta = 0.67$ to 220% for $\beta = 1.40$.

Furthermore, as with the CMS-MTJs, the TMR ratios of CMG-MTJs at both 4.2 K and RT increased with increasing β even beyond $\beta = 1.0$, where $\beta = 1.0$ corresponds to the Co:Mn ratio of 2:1, and the maximum TMR ratios of 650% at 4.2 K and 220% at RT were obtained for $\beta = 1.40$ in the β range up to 1.40 used in this study.

3.4. Saturation magnetization of nonstoichiometric $Co_2Mn_\beta Ge_{0.38}$ thin films

Figure 5(a) shows experimentally obtained μ_s values for $Co_2Mn_\beta Ge_{0.38}$ thin films at 10 K as a function of β, along with $Z_t - 24$, where Z_t is the total valence electron number per formula unit provided by the formula unit model for $Co_2Mn_\beta Ge_{0.38}$ discussed in section 4.3. The experimental μ_s values for β ranging from 0.67 to 1.40 were larger than 5.0 μ_B/f.u., which is the value theoretically predicted by the Slater–Pauling rule for stoichiometric, half-metallic Co_2MnGe [7]. The experimental μ_s values increased with increasing β from 6.06 μ_B/f.u. for $\beta = 0.67$ to 6.63 μ_B/f.u. for $\beta = 1.40$. This β dependence of μ_s is discussed in section 4.3 on the basis of a formula unit model that includes antisite defects.

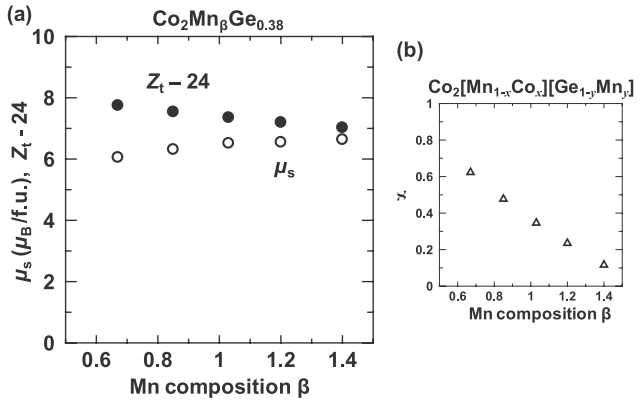

Figure 5. (a) Experimentally obtained μ_s values (open circles) for $Co_2Mn_\beta Ge_{0.38}$ thin films at 10 K and $Z_t - 24$ (solid circles) as a function of β ranging from $\beta = 0.67$ to 1.40, where Z_t is the total valence electron number per formula unit provided by the formula unit model $Co_2[Mn_{1-x}Co_x][Ge_{1-y}Mn_y]$ for $Co_2Mn_\beta Ge_{0.38}$ with $\beta < 1.62$. (b) Co_{Mn} antisite ratios x provided by the formula unit model $Co_2[Mn_{1-x}Co_x][Ge_{1-y}Mn_y]$ for $Co_2Mn_\beta Ge_{0.38}$ with $\beta < 1.62$ as a function of β ranging from $\beta = 0.67$ to 1.40.

4. Discussion

4.1. Effect of defects on TMR ratios at low temperatures

Now we discuss the possible origin of the dependence of the TMR ratio, or equivalently of G_P/G_{AP}, on the Mn composition in CMS-MTJs and CMG-MTJs. In this section, we discuss the tunnelling mechanism at low temperatures and low bias voltages. Here, low temperatures mean that thermal energy k_BT is much lower than the minimum magnon excitation energy ($\hbar\omega_0$), and low bias voltages mean that eV is lower than $\hbar\omega_0$. Considering that the characteristic energy for magnon excitation was typically 4 meV for fully epitaxial CMS-MTJs, as reported in our previous papers [27, 28], $V = 1$ meV used to measure the TMR ratio at 4.2 K was lower than the magnon excitation energy. Thus, we can ignore tunnelling processes that include spin-flip scattering via magnons excited thermally or excited by hot electrons in the electrodes at 4.2 K. Then, the main tunnelling paths for AP at 4.2 K and $V = 1$ mV for MTJs with high spin polarizations to be taken into consideration include (1) a tunnelling path from the majority-spin band in the emitter to minority-spin in-gap states in the bulk region of the collector directly or through minority-spin interface states in the interfacial region of the collector facing a MgO barrier and (2) a tunnelling path from minority-spin in-gap states in the bulk region of the emitter to the majority-spin band in the collector directly or through minority-spin interface states in the interfacial region of the emitter facing a MgO barrier. Therefore, the main factor that determines G_{AP} at low T and low V is the density of minority-spin in-gap states at E_F ($D_{gs}(E_F)$), and the G_{AP} is proportional to $D_{gs}(E_F)$, i.e.,

$$G_{AP}\ (\text{at low } T \text{ and low } V) \propto D_{gs}(E_F). \qquad (1)$$

Therefore, the TMR ratio in potentially half-metallic Co_2YZ-based MTJs at low T and low V is crucially dependent on $D_{gs}(E_F)$ and increases with decreasing $D_{gs}(E_F)$. For a more rigorous treatment, we must take into consideration the influence of coherent tunnelling (conservation of the electron wavevector parallel to the plane), and $D_{gs}(E_F)$ in equation (1) should be replaced by the partial density of minority-spin in-gap states at E_F for which the tunnelling probability is higher due to the coherent tunnelling effect.

Nonstoichiometry in Co_2YZ generally induces defects. The effect of defects on half-metallicity for Co_2YZ has been investigated theoretically by first principles calculations [35–41]. Picozzi *et al* theoretically predicted that the Co_{Mn} antisites induce minority-spin in-gap states around E_F, resulting in reduced spin polarizations, while the Mn_{Co} antisites retain the half-metallic character [35]. On the other hand, Galanakis *et al* theoretically investigated the effect of disorder between Mn atoms and Si atoms for the $Co_2Mn_{1+x}Si_{1-x}$ system for both $x < 0$ (Mn-deficient side) and $x > 0$ (Mn-rich side) [37]. They reported that substituting Si for Mn, which is likely to occur for the Mn-deficient side, induces states just at the bottom edge of the minority-spin half-metal gap, while substituting Mn for Si, which is likely to occur for the Mn-rich side, pushes the unoccupied minority-spin states even higher in energy and the half-metal gap becomes wider. Therefore, the disorder between Mn and Si atoms does not induce minority-spin in-gap states around E_F, and half-metallicity is thus retained. Furthermore, note that the Mn-rich side in the $Co_2Mn_{1+x}Si_{1-x}$ system is more favourable than the Mn-deficient side for stable half-metallicity because the half-metal gap is wider for the Mn-rich side.

Next, we consider possible defects induced by Mn-deficient nonstoichiometry in $Co_2Mn_\alpha Si$ ($\alpha < 1$). According to the theoretically predicted formation energies of various defects induced in CMS [35, 41], Si_{Mn} antisites are likely to be induced for the range $\alpha < 1$. This is because a Si_{Mn} antisite has much lower formation energy than a Co_{Mn} antisite and a vacancy at a Mn site. If only Si_{Mn} antisites are induced, however, in the prepared $Co_2Mn_\alpha Si$ thin film having a Co:Si ratio almost of 2:1, vacancies will be formed at Si sites. However, this possibility would be quite low because a Co_{Mn} antisite has much lower formation energy than a vacancy at a Si site. Thus, it is most likely that Si_{Mn} antisites are induced along with Co_{Mn} antisites for the range $\alpha < 1$, resulting in the formula unit model $Co_2[Mn_{1-x-y}Co_xSi_y]Si$, where $[Mn_{1-x-y}Co_xSi_y]$ represents the nominal Mn site. The Co:Mn:Si ratio in $Co_2[Mn_{1-x-y}Co_xSi_y]Si$ must be equal to that in the representation of $Co_2Mn_\alpha Si$ with a given α value. From this requirement, the values of x and y are determined. According to this model, the Co_{Mn} antisite ratio x decreases with increasing α in the range $\alpha < 1.0$ from $x = 0.17$ for $\alpha = 0.69$ to $x = 0$ for $\alpha = 1.0$.

Similarly, Mn_{Co} antisites are likely to be induced for the range $\alpha > 1$. This is because a Mn_{Co} antisite has much lower formation energy than other defects, including a vacancy at a Co site, a Mn_{Si} antisite, and a vacancy at a Si site. If only Mn_{Co} antisites are induced, however, vacancies will be formed at Si sites. However, this possibility would be quite low because a Mn_{Si} antisite has much lower formation energy than a vacancy at a Si site. Thus, it is most likely that Mn_{Co} antisites are induced along with Mn_{Si}

antisites for the range $\alpha > 1$, resulting in the formula unit model $[Co_{2-z}Mn_z]Mn[Si_{1-u}Mn_u]$, where $[Co_{2-z}Mn_z]$ and $[Si_{1-u}Mn_u]$ represent the nominal Co and Si sites, respectively.

Given these considerations, we discuss the effect of defects on minority-spin in-gap states. For Mn-deficient $Co_2Mn_\alpha Si$ thin films ($\alpha < 1$), it is likely that Co_{Mn} antisites are induced, as discussed above. Note that Co_{Mn} antisites are most harmful for the half-metallicity of CMS and CMG, whereas Si_{Mn} and Mn_{Si} antisites do not affect the half-metallicity at all, as discussed above. Therefore, the observed lower TMR ratio or equivalently lower G_P/G_{AP} for MTJs with Mn-deficient Co_2MnSi electrodes at 4.2 K (figures 2(b) and 3, respectively) would be due to induced Co_{Mn} antisites, which result in increased $D_{gs}(E_F)$ and thereby lead to the increased G_{AP}.

With increasing α beyond 1, where $\alpha = 1$ corresponds to the Co:Mn ratio of 2:1, Mn_{Co} antisites would be induced, while detrimental Co_{Mn} antisites would be suppressed, as discussed above. Thus, the observed higher TMR ratio or equivalently higher G_P/G_{AP} for MTJs with Mn-rich Co_2MnSi electrodes would be due to suppressed Co_{Mn} antisites, which result in decreased $D_{gs}(E_F)$ and thereby lead to the decreased G_{AP}.

In this section, we have mainly discussed the dependence of the TMR ratio of CMS-MTJs on the Mn composition of Co_2MnSi electrodes. The discussion is also applicable to CMG-MTJs, considering that the effect of defects in Co_2MnGe hosts on the half-metallic gap structure is essentially the same, as suggested by the theoretical calculations [35]. The possible defects induced in nonstoichiometric, Ge-deficient $Co_2Mn_\beta Ge_{0.38}$ thin films are discussed in detail in section 4.3.

Note that the proposed formula unit models for $\alpha < 1$ and $\alpha > 1$ for $Co_2Mn_\alpha Si$ both provide the Co_{Mn} antisite ratio $x = 0$ for $\alpha \geqslant 1.0$. This is because the models are based on the formation energies of various kinds of defects in the thermal equilibrium state. The increase in the TMR ratio or equivalently that of G_P/G_{AP} with increasing α beyond $\alpha = 1$ for MTJs with CMS electrodes, however, suggests that Co_{Mn} antisites were induced in CMS thin films even for $\alpha \geqslant 1.0$, indicating that CMS films prepared by sputtering at RT and subsequent annealing at around 500–600 °C do not reach a thermal equilibrium state. Our experimental findings indicate, however, that the concentration of detrimental Co_{Mn} antisites decreases with increasing α beyond $\alpha = 1$ and hence the density of minority-spin in-gap states is reduced in Co_2MnSi electrodes. For the $Co_2Mn_\beta Ge_{0.38}$ thin films, we must also take into consideration that the Ge composition was strongly deficient with respect to the Co composition (see section 4.3).

4.2. Effect of defects on TMR ratios at room temperature

For tunnelling processes for AP at elevated temperatures, where k_BT is comparable or larger than $\hbar\omega_0$, we must take into consideration tunnelling processes for AP that associate spin-flip scattering in the emitter or collector electrode via thermally excited magnons, including the following processes: (1) electrons are spin-flip scattered in the emitter from the majority-spin band to minority-spin in-gap states in the bulk region or minority-spin interface states by thermally excited magnons and then electrons tunnel to the majority-spin band of the collector and (2) electrons tunnel from the majority-spin band of the emitter to minority-spin interface states or minority-spin in-gap states in the bulk region of the collector and then electrons are spin-flip scattered in the collector to the majority-spin band by thermally excited magnons. This model takes into consideration both minority-spin interface states [27, 43] and minority-spin in-gap states in the bulk region of electrodes. These tunnelling processes increase G_{AP} (or equivalently decrease R_{AP}) with increasing T because the density of thermally excited magnons increases with increasing T.

Note that minority-spin in-gap states in the bulk region and minority-spin interface states are involved in these tunnelling processes. Therefore, G_{AP} at finite T and low V would be proportional to the total density of minority-spin in-gap states at E_F that is the sum of the density of minority-spin interface states at E_F (D_{if} (E_F)) and D_{gs} (E_F), and G_{AP} at finite T is expressed as

$$G_{AP}\ (\text{at finite } T \text{ and low } V) \propto [D_{if}(E_F) + D_{gs}(E_F)] \times [T\text{-dependent term}], \quad (2)$$

where the T-dependent term represents the effect of spin-flip scattering via thermally excited magnons. Here, we ignored the effect of magnons excited by hot electrons due to the finite V at RT. The excess energy of $e|V|$ at RT for tunnelling electrons arising from the finite V of 5 mV used for the measurements at RT may excite magnons in the collector region, but the TMR ratios measured at $V = 5$ mV were less than 1% lower than those measured at $V = 1$ mV ($e|V| = 1$ meV is less than the characteristic magnon excitation energy of ∼4 meV). This means that the effect of magnons excited by hot electrons with excess energy of up to 5 mV at RT can be ignored at RT in comparison with the effect of thermally excited magnons at RT ($k_BT \sim 26$ meV). In this sense, we could regard V of up to 5 mV used here as being a low voltage. In a more rigorous treatment, however, the term D_{if} (E_F) + $D_{gs}(E_F)$ in equation (2) should also be replaced by the partial density of minority-spin in-gap states at E_F, including that of minority-spin interface states, for which the tunnelling probability is higher due to the coherent tunnelling effect.

The increase in G_P/G_{AP} with increasing α for an α range of 0.69–1.29 at RT (figure 4(b)) can be explained by the decrease in G_{AP} caused by the decrease in the total density of minority-spin in-gap states at E_F, i.e., D_{if} (E_F)+$D_{gs}(E_F)$. The minority-spin interface states at E_F may include (1) intrinsic interface states investigated theoretically [44] and (2) extrinsic interface states influenced by structural defects at the interface. Therefore, D_{if} (E_F), like $D_{gs}(E_F)$, is a quantity that changes with α. Although we could not separate the contributions of $D_{gs}(E_F)$ and $D_{if}(E_F)$ to G_{AP} at RT, it is certain that $D_{gs}(E_F)$ plays a role in determining the dependence of G_P/G_{AP} on α at RT. As discussed in section 4.1, $D_{gs}(E_F)$ decreases with the change from Co_{Mn} antisites for the Mn-deficient side to Mn_{Co} antisites for the Mn-rich side, resulting in the increase in G_P/G_{AP} for α up to 1.29 also at RT through the term of $D_{gs}(E_F)$ in equation (2).

4.3. Defects induced in nonstoichiometric, Ge-deficient $Co_2Mn_\beta Ge_{0.38}$

We now discuss possible defects induced in the prepared nonstoichiometric, Ge-deficient $Co_2Mn_\beta Ge_{0.38}$ films. Note that the Co:Ge ratio in the prepared CMG films was 2:0.38, i.e., the Ge ratio was strongly deficient with respect to the Co ratio. According to the theoretically predicted formation energies of various kinds of defects for Co_2MnSi [41], with the assumption that the relative magnitude of these formation energies for Co_2MnGe is essentially the same as that for Co_2MnSi, we introduce a formula unit composition model for strongly Ge-deficient CMG films with $\beta < \beta_c = 1.62$ as $Co_2[Mn_{1-x}Co_x][Ge_{1-y}Mn_y]$, where $[Mn_{1-x}Co_x]$ and $[Ge_{1-y}Mn_y]$ represent the nominal Mn and Ge sites, respectively. The detailed reasons for this model are as follows: for Ge sites, Mn_{Ge} antisites, where a Ge site is replaced with a Mn atom, are likely to be induced because a Mn_{Ge} antisite has much lower formation energy than a vacancy at a Ge site and a Co_{Ge} antisite [41]. Thus, Ge sites are fully occupied by the normal Ge atoms and Mn_{Ge} antisites. For Mn sites, Co_{Mn} antisites are likely to be induced because a Co_{Mn} antisite has lower formation energy than a vacancy at a Mn site [41]. Thus, the normal Mn atoms and Co_{Mn} antisites should occupy Mn sites. The Co:Mn:Ge ratio in $Co_2[Mn_{1-x}Co_x][Ge_{1-y}Mn_y]$ must be also equal to that in the representation of $Co_2Mn_\beta Ge_{0.38}$ with a given β value. From this requirement, the values of x and y are determined. This model provides the total number of valence electrons per f.u. (Z_t) and the Co_{Mn} site ratio x for a given β ($< \beta_c$). The numbers of $Z_t - 24$ are plotted in figure 5(a) and the x values are plotted in figure 5(b), both as a function of β. This model provides respective formula units ranging from $Co_2[Mn_{0.377}Co_{0.623}][Ge_{0.498}Mn_{0.502}]$ (where x is 0.62 and $Z_t = 31.75$) for $Co_2Mn_{0.67}Ge_{0.38}$ to $Co_2[Mn_{0.884}Co_{0.116}][Ge_{0.402}Mn_{0.598}]$ (where x is 0.12 and $Z_t = 31.03$) for $Co_2Mn_{1.40}Ge_{0.38}$. Even at $\beta = 1.03$, for which the Co:Mn ratio is close to 2:1, the model provides a formula unit of $Co_2[Mn_{0.654}Co_{0.346}][Ge_{0.446}Mn_{0.554}]$ that features a still high x value of 0.35 for $Co_2Mn_{1.03}Ge_{0.38}$. This is because the Ge ratio is strongly deficient for $Co_2Mn_\beta Ge_{0.38}$. For $\beta = \beta_c = 1.62$, the model predicts a formula unit of $Co_2Mn[Ge_{0.38}Mn_{0.62}]$, where x becomes zero. Importantly, the ratio x of the detrimental Co_{Mn} antisite at the Mn site considerably decreases with increasing β from $x = 0.62$ for $\beta = 0.67$ to $x = 0.12$ for $\beta = 1.40$ with this formula unit model. Thus, this formula unit model derived by taking into account the formation energies of various defects at the thermal equilibrium state can reasonably explain the β dependence of the TMR ratio observed for CMG-MTJs with $Co_2Mn_\beta Ge_{0.38}$ electrodes, i.e., the observed increase in the TMR ratio with increasing β up to 1.40 is ascribed to a decrease in the Co_{Mn} antisite ratio x, which causes a reduced density of minority-spin in-gap states around E_F. If we take into account that the $Co_2Mn_\beta Ge_{0.38}$ films were prepared by sputtering and subsequent annealing around 500 °C, the films probably did not reach a thermal equilibrium state. Thus, the Co_{Mn} antisite ratio $x = 0.12$ for $\beta = 1.40$ estimated by this formula unit model (figure 5(b)) should be regarded as the lower bound for $\beta = 1.40$ and the realistic x value for $\beta = 1.40$ should be higher than this value.

We now examine the validity of this formula unit model by comparing the experimental β dependence of μ_s at 10 K of $Co_2Mn_\beta Ge_{0.38}$ films with Slater–Pauling behaviour of μ_s, which is applicable for half-metallic Heusler alloys and predicts $\mu_s = Z_t - 24$ (μ_B/f.u.) for half-metallic Co_2YZ alloys [7]. Although the experimental μ_s values were much smaller than the Slater Pauling values of $Z_t - 24$ for $\beta < 1.0$, they approached the values given by $Z_t - 24$ with increasing β up to 1.40, as shown in figure 5(a), and the experimental $\mu_s = 6.63$ μ_B/f.u. for $\beta = 1.40$ is close to the Slater–Pauling value of 7.03 μ_B/f.u. for $\beta = 1.40$. These behaviours of the experimental μ_s are consistent with the formula unit model. First, the larger difference between the experimental μ_s and $Z_t - 24$ for $\beta < 1.0$ is reasonable because the large Co_{Mn} antisite ratio for $\beta < 1.0$ predicted by the formula unit model results in a certain density of minority-spin in-gap states around E_F [35], leading to the Slater–Pauling μ_s value not being good approximation. However, the difference between the experimental μ_s and $Z_t - 24$ deceases with increasing β up to 1.40 because the Co_{Mn} antisite ratio x decreases with increasing β beyond $\beta = 1.0$ according to the formula unit model. Because of the relatively small value of $x = 0.12$ for $\beta = 1.40$, the experimental μ_s of $Co_2Mn_\beta Ge_{0.38}$ with $\beta = 1.40$ was in relatively good agreement (within 6%) with the Slater–Pauling μ_s for $\beta = 1.40$. The difference between these two values, i.e., the smaller experimental μ_s than the Slater–Pauling μ_s for $\beta = 1.40$ is reasonable if we take into account that the $Co_2Mn_\beta Ge_{0.38}$ film with $\beta = 1.40$ still contains at least the 12% Co_{Mn} antisite ratio at a Mn site. In summary, it was shown that the formula unit model based on the formation energies of various kinds of defects reasonably explains the observed dependence of μ_s on β. This finding supports our interpretation that the Mn composition dependence of the TMR ratio observed universally for both CMS-MTJs and CMG-MTJs is due to suppressed minority-spin in-gap states around E_F which are caused by the decreased Co_{Mn} antisites in Mn-rich CMS and CMG electrodes.

5. Conclusion

We investigated the TMR characteristics of CMS/MgO/CMS-MTJs and CMG/MgO/CMG-MTJs fabricated with various Mn compositions α and β in $Co_2Mn_\alpha Si$ and $Co_2Mn_\beta Ge_{0.38}$ electrodes. We obtained higher TMR ratios for CMS/MgO/CMS-MTJs with Mn-rich Co_2MnSi electrodes and for CMG/MgO/CMG-MTJs with Mn-rich $Co_2MnGe_{0.38}$ electrodes and we observed high TMR ratios of 1135% at 4.2 K and 236% at RT for MTJs with Mn-rich $Co_2Mn_\alpha Si$ electrodes with $\alpha = 1.29$. The observed lower TMR ratio for MTJs with Mn-deficient Co_2MnSi or $Co_2MnGe_{0.38}$ electrodes was explained by induced Co_{Mn} antisites, which resulted in an increased density of minority-spin in-gap states around E_F and thereby led to increased tunnel conductance for AP. On the other hand, the observed higher TMR ratio for MTJs with Mn-rich Co_2MnSi or $Co_2MnGe_{0.38}$ electrodes was explained by suppressed Co_{Mn} antisites, which caused

a reduced density of minority-spin in-gap states around E_F and thereby led to decreased tunnel conductance for AP. It was shown that the picture of suppressed Co_{Mn} antisites with increasing Mn composition in $Co_2Mn_\alpha Si$ and $Co_2Mn_\beta Ge_{0.38}$ films is consistent with the formula unit composition models introduced by taking into account the theoretical formation energies of various kinds of defects induced in Co_2MnSi and Co_2MnGe. It was found that the formula unit model for Ge-deficient $Co_2Mn_\beta Ge_{0.38}$ films qualitatively explains the observed β dependence of the saturation magnetization per formula unit at 10 K, supporting the validity of the formula unit models for $Co_2Mn_\alpha Si$ and $Co_2Mn_\beta Ge_{0.38}$ films. In conclusion, our experimental findings suggest that the density of minority-spin in-gap states can be reduced by appropriately controlling defects in Co_2MnSi and Co_2MnGe electrodes. Nonstoichiometry is inevitable, to various degrees, in Co_2YZ thin films, which are mostly prepared by magnetron sputtering. Our findings, however, suggest that detrimental Co_{Mn} antisites can be suppressed by preparing Co_2MnZ films with a Mn-rich composition.

Acknowledgments

We thank S Hirata and H-x Liu for experimental help. This work was partly supported by Grants-in-Aid for Scientific Research (A) (Grant No. 20246054) and (B) (Grant No. 21360140) and a Grant-in-Aid for Scientific Research on Priority Area 'Creation and control of spin current' (Grant No. 19048001) from the Ministry of Education, Culture, Sports, Science and Technology, Japan, and by the Strategic International Cooperative Program of the Japan Science and Technology Agency (JST).

References

[1] Wolf S A, Awschalom D D, Buhrman R A, Daughton J M, von Molnár S, Roukes M L, Chtchelkanova A Y and Treger D M 2001 *Science* **294** 1488
[2] Žutić I, Fabian J and Das Sarma S 2004 *Rev. Mod. Phys.* **76** 323
[3] de Groot R A, Mueller F M, van Engen P G and Buschow K H J 1983 *Phys. Rev. Lett.* **50** 2024
[4] Felser C, Fecher G H and Balke B 2007 *Angew. Chem. Int. Edn* **46** 668
[5] Ishida S, Fujii S, Kashiwagi S and Asano S 1995 *J. Phys. Soc. Japan* **64** 2152
[6] Picozzi S, Continenza A and Freeman A J 2002 *Phys. Rev.* B **66** 094421
[7] Galanakis I, Dederichs P H and Papanikolaou N 2002 *Phys. Rev.* B **66** 174429
[8] Webster P J 1971 *J. Phys. Chem. Solids* **32** 1221
[9] Inomata K, Okamura S, Goto R and Tezuka N 2003 *Japan. J. Appl. Phys.* **42** L419
[10] Kämmerer S, Thomas A, Hütten A and Reiss G 2004 *Appl. Phys. Lett.* **85** 79
[11] Kubota H, Nakata J, Oogane M, Ando Y, Sakuma A and Miyazaki T 2004 *Japan. J. Appl. Phys.* **43** L984
[12] Marukame T, Kasahara T, Matsuda K-I, Uemura T and Yamamoto M 2005 *Japan. J. Appl. Phys.* **44** L521
[13] Ishikawa T, Marukame T, Kijima H, Matsuda K-I, Uemura T, Arita M and Yamamoto M 2006 *Appl. Phys. Lett.* **89** 192505
[14] Sakuraba Y, Hattori M, Oogane M, Ando Y, Kato H, Sakuma A, Miyazaki T and Kubota H 2006 *Appl. Phys. Lett.* **88** 192508
[15] Tezuka N, Ikeda N, Mitsuhashi F and Sugimoto S 2009 *Appl. Phys. Lett.* **94** 162504
[16] Yakushiji K, Saito K, Mitani S, Takanashi K, Takahashi Y K and Hono K 2006 *Appl. Phys. Lett.* **88** 222504
[17] Furubayashi T, Kodama K, Sukegawa H, Takahashi Y K, Inomata K and Hono K 2008 *Appl. Phys. Lett.* **93** 122507
[18] Sakuraba Y, Iwase T, Saito K, Mitani S and Takanashi K 2009 *Appl. Phys. Lett.* **94** 012511
[19] Nikolaev K, Kolbo P, Pokhil T, Peng X, Chen Y, Ambrose T and Mryasov O 2009 *Appl. Phys. Lett.* **94** 222501
[20] Dong X Y, Adelmann C, Xie J Q, Palmstrøm C J, Lou X, Strand J, Crowell P A, Barnes J-P and Petford-Long A K 2005 *Appl. Phys. Lett.* **86** 102107
[21] Hickey M C, Damsgaard C D, Farrer I, Holmes S N, Husmann A, Hansen J B, Jacobsen C S, Ritchie D A, Lee R F, Jones G A C and Pepper M 2005 *Appl. Phys. Lett.* **86** 252106
[22] Yamamoto M, Marukame T, Ishikawa T, Matsuda K, Uemura T and Arita M 2006 *J. Phys. D: Appl. Phys.* **39** 824
[23] Marukame T, Ishikawa T, Hakamata S, Matsuda K-I, Uemura T and Yamamoto M 2007 *Appl. Phys. Lett.* **90** 012508
[24] Taira T, Ishikawa T, Itabashi N, Matsuda K-I, Uemura T and Yamamoto M 2009 *J. Phys. D: Appl. Phys.* **42** 084015
[25] Marukame T, Ishikawa T, Hakamata S, Matsuda K-I, Uemura T and Yamamoto M 2007 *IEEE Trans. Magn.* **43** 2782
[26] Ishikawa T, Hakamata S, Matsuda K-I, Uemura T and Yamamoto M 2008 *J. Appl. Phys.* **103** 07A919
[27] Ishikawa T, Itabashi N, Taira T, Matsuda K-I, Uemura T and Yamamoto M 2009 *Appl. Phys. Lett.* **94** 092503
[28] Ishikawa T, Itabashi N, Taira T, Matsuda K-I, Uemura T and Yamamoto M 2009 *J. Appl. Phys.* **105** 07B110
[29] Saito T, Katayama T, Ishikawa T, Yamamoto M, Asakura D and Koide T 2007 *Appl. Phys. Lett.* **91** 262502
[30] Saito T, Katayama T, Emura A, Sumida N, Matsuoka N, Ishikawa T, Uemura T, Yamamoto M, Asakura D and Koide T 2008 *J. Appl. Phys.* **103** 07D712
[31] Butler W H, Zhang X-G, Schulthess T C and MacLaren J M 2001 *Phys. Rev.* B **63** 054416
[32] Mathon J and Umerski A 2001 *Phys. Rev.* B **63** 220403(R)
[33] Miura Y, Uchida H, Oba Y, Nagao K and Shirai M 2007 *J. Phys.: Condens. Matter* **19** 365228
[34] Kawagishi S, Uemura T, Imai Y, Matsuda K-I and Yamamoto M 2008 *J. Appl. Phys.* **103** 07A703
[35] Picozzi S, Continenza A and Freeman A J 2004 *Phys. Rev.* B **69** 094423
[36] Miura Y, Nagao K and Shirai M 2004 *Phys. Rev.* B **69** 144413
[37] Galanakis I, Özdoğan K, Aktaş B and Şaşıoğlu E 2006 *Appl. Phys. Lett.* **89** 042502
[38] Özdoğan K, Galanakis I, Şaşıoğlu E and Aktaş B 2007 *Solid State Commun.* **142** 492
[39] Özdoğan K, Şaşıoğlu E and Galanakis I 2007 *Phys. Status Solidi (RRL)* **1** 184
[40] Galanakis I, Özdoğan K, Şaşıoğlu E and Aktaş B 2008 *Phys. Status Solidi* a **205** 1036
[41] Hülsen B, Scheffler M and Kratzer P 2009 *Phys. Rev.* B **79** 094407
[42] Nakatani T M, Takahashi Y K, Ishikawa T, Yamamoto M and Hono K 2010 *J. Magn. Magn. Mater.* **322** 357
[43] Mavropoulos Ph, Ležaić M and Blügel S 2005 *Phys. Rev.* B **72** 174428
[44] Miura Y, Uchida H, Oba Y, Abe K and Shirai M 2008 *Phys. Rev.* B **78** 064416